Frequency-Adaptive Observer to Extract AC-Coupled Signals for Grid Synchronization

Yongsoon Park, *Member, IEEE*, Hyeon-Sik Kim, *Member, IEEE*, and Seung-Ki Sul, *Fellow, IEEE*

***Abstract*—In three-phase grids, the grid synchronization has been widely discussed with mainly focusing on the mitigation of low-order harmonics and unbalances. In this paper, the elimination of a dc bias is also considered in the process of the grid synchronization. Because the proposed method is based on a frequency-adaptive observer, it can maintain its performances even if the fundamental frequency is changed. The state equation is newly established for the observer, and its gains are discussed in terms of their influences to the filtering performances. The effectiveness of the proposed method is assessed with various simulations and experiments.**

***Index Terms*—Adaptive observer, dc rejection, grid synchronization.**

I. Introduction

THE power transfer between a converter and an ac grid can be modulated by adjusting not only the converter current's magnitude but also its relative phase difference to the grid voltage. That is, there exists a reference voltage for the power transfer, which is commonly called as positive-sequence voltage [1]. The grid synchronization is to detect this positive-sequence voltage from the real grid voltage, which can include some distortions such as harmonics, unbalances, and glitches.

Phase locked loop (PLL) is a well-known principle for the grid synchronization [2]. There are numerous variations of the basic PLL in order to filter out the grid distortions [2]–[21]. However, even if they seem to be different in their implementations, they aim at the same purpose: the clear detection of positive-sequence voltage. Thus, they cannot help having similarities in functional aspects. Namely, the characteristics of notch or low-pass filtering are commonly employed [3]. Then, it becomes important for the grid synchronization how these diverse functions can be integrated into a simpler structure.

In the literature, a PLL method was proposed in the basis of a preprocessing observer (SOAP-PLL) [9]. First of all, this method is effective for the compact integration of the filtering functions by means of a state equation for the observer. Furthermore, every filtering response can be explicitly understood through the transfer functions of the observer. This feature would be very helpful if the filtering responses need to be modified according to grid conditions. For these reasons, the proposed method in this paper is also based on an observer.

The proposed method was intended to be more versatile. First, the function to generate a quadrature voltage, such as second-order generalized integrator (SOGI), is essential [10]. Although a PLL can be implemented in the synchronously rotating frame (SRF-PLL) with three-phase voltage, the derivatives of SRF-PLL cannot be easily applied to single-phase grids. This is because they need a pair of voltages showing a phase difference by 90 degrees. In addition, a quadrature voltage could be utilized to extract positive-sequence voltage easily in three-phase grids. Thus, the proposed method has to naturally generate the quadrature voltage. Second, dc biases should be considered for completeness in the grid synchronization because it can be observed in diverse situations such as the process of analog to digital conversions, grid faults, and dc injection from distributed generation systems [11]–[20]. A dc bias should be eliminated carefully in the process of grid synchronization because angle and frequency estimations would be oscillated with the dc bias. It is difficult to filter out dc biases through conventional low-pass filtering due to the characteristics of dc. These two points are reflected in establishing the state equation of the proposed observer.

The assessment of the proposed method is carried out through the comparisons with the conventional frequency-adaptive methods, SOAP-PLL and dual SOGI frequency locked loop (DSOGI-FLL) [9], [10]. This is because the grid frequency can fluctuate in real time depending on its circumstances. Through simulation and experimental results, the proposed method is evaluated with respect to harmonic filtering, dc and unbalance rejections, and frequency adaptiveness.

II. Frequency-Adaptive Observer

A. State Equation and Transfer Functions

As mentioned earlier, it is required for the proposed observer to generate a quadrature component and to eliminate a dc bias from an original signal. Thus, the observer design starts by defining these components as state variables so that the observer estimates its state variables [22]. Every state variable is then defined as follows:

$$\begin{bmatrix} \mathrm{x} \\ \mathrm{y} \\ \mathrm{z} \end{bmatrix} = \begin{bmatrix} V_m \sin\theta \\ -V_m \cos\theta \\ \mathrm{x} + \mathrm{D} \end{bmatrix} \tag{1}$$

Manuscript received February 19, 2016; revised June 6, 2016; accepted August 7, 2016. Date of publication August 30, 2016; date of current version January 18, 2017. Paper 2016-IPCC-0190.R1, presented at the 2015 International Conference on Power Electronics and ECCE Asia, Seoul, South Korea, June 1–5, and approved for publication in the IEEE TRANSACTIONS ON INDUSTRY APPLICATIONS by the Industrial Power Converter Committee of the IEEE Industry Applications Society.

Y. Park is with Gwangju Institute of Science and Technology, Gwangju 61005, South Korea (e-mail: yongsoon@gist.ac.kr).

H.-S. Kim and S.-K. Sul are with the Department of Electrical and Computer Engineering, Seoul National University, Seoul 08826, South Korea (e-mail: hyeonsik@eepel.snu.ac.kr; sulsk@plaza.snu.ac.kr).

Color versions of one or more of the figures in this paper are available online at http://ieeexplore.ieee.org.

Digital Object Identifier 10.1109/TIA.2016.2604299

where "z" is the original signal including ac and dc components. Specifically, "x" is the ac component, whose phase is θ, and "D" is the dc component. When compared to "x," the component "y" has the same magnitude, V_m, while lagging by 90°.

Among the variables in (1), because the derivative of "D" is deemed null, the derivative of "z" is identical to that of "x". In result, "D" is selected as one of the state variables instead of "z." Then, the state-equation is finally established as follows:

$$\frac{d}{dt}\begin{bmatrix}\mathrm{x}\\ \mathrm{y}\\ \mathrm{D}\end{bmatrix} = \begin{bmatrix}0 & -\omega & 0\\ \omega & 0 & 0\\ 0 & 0 & 0\end{bmatrix}\begin{bmatrix}\mathrm{x}\\ \mathrm{y}\\ \mathrm{D}\end{bmatrix} = A_e\begin{bmatrix}\mathrm{x}\\ \mathrm{y}\\ \mathrm{D}\end{bmatrix}, \quad \text{(2-a)}$$

$$z = \begin{bmatrix}1 & 0 & 1\end{bmatrix}\begin{bmatrix}\mathrm{x}\\ \mathrm{y}\\ \mathrm{D}\end{bmatrix} = C_e\begin{bmatrix}\mathrm{x}\\ \mathrm{y}\\ \mathrm{D}\end{bmatrix} \quad \text{(2-b)}$$

where ω is denoted as the fundamental frequency and corresponds to the derivative of θ.

By considering A_e and C_e in (2), the observability of the state equation can be determined. Because the rank of O_e in (3) corresponds to full column rank, the state equation is regarded as observable, and a Luenberger observer would be designed according to (4):

$$\mathrm{rank}(O_e) = \mathrm{rank}\begin{bmatrix}C_e\\ C_eA_e\\ C_eA_e^2\end{bmatrix} = 3, \quad (3)$$

$$\frac{d}{dt}\begin{bmatrix}\hat{\mathrm{x}}\\ \hat{\mathrm{y}}\\ \hat{\mathrm{D}}\end{bmatrix} = \begin{bmatrix}0 & -\omega & 0\\ \omega & 0 & 0\\ 0 & 0 & 0\end{bmatrix}\begin{bmatrix}\hat{\mathrm{x}}\\ \hat{\mathrm{y}}\\ \hat{\mathrm{D}}\end{bmatrix} + \begin{bmatrix}k_1\\ k_2\\ k_3\end{bmatrix}\{\mathrm{z} - (\hat{\mathrm{x}} + \hat{\mathrm{D}})\} \quad (4)$$

where the hat "^" over variable means estimated one.

After replacing the derivative operator "d/dt" with the Laplace operator "s," the estimated state variables are expressed with respect to "z" that is the original signal and only measurable, as shown in

$$\begin{bmatrix}\hat{\mathrm{x}}\\ \hat{\mathrm{y}}\\ \hat{\mathrm{D}}\end{bmatrix} = \begin{bmatrix}\mathrm{s}+k_1 & \omega & k_1\\ -\omega+k_2 & \mathrm{s} & k_2\\ k_3 & 0 & \mathrm{s}+k_3\end{bmatrix}^{-1}\begin{bmatrix}k_1\mathrm{z}\\ k_2\mathrm{z}\\ k_3\mathrm{z}\end{bmatrix}. \quad (5)$$

Then, the transfer functions from the original signal to each variable can be derived as follows:

$$\frac{\hat{x}}{z} = d(s) = \frac{s^2k_1 - \mathrm{s}\omega k_2}{s^3 + s^2(k_1+k_3) + \mathrm{s}\omega(\omega - k_2) + k_3\omega^2} \quad \text{(6-a)}$$

$$\frac{\hat{y}}{z} = q(s) = \frac{s^2k_2 + \mathrm{s}\omega k_1}{s^3 + s^2(k_1+k_3) + \mathrm{s}\omega(\omega - k_2) + k_3\omega^2} \quad \text{(6-b)}$$

$$\frac{\hat{D}}{z} = n(s) = \frac{k_3(s^2+\omega^2)}{s^3 + s^2(k_1+k_3) + \mathrm{s}\omega(\omega - k_2) + k_3\omega^2}. \quad \text{(6-c)}$$

The properties of the proposed observer can be explained with the closed formats by virtue of the state equation as intended. This is a distinctive feature of the proposed method in that its integrated filtering property can be simply understood without any approximation.

B. Observer Gain Settings

The observer gains of k_1, k_2, and k_3 can be determined by pole placements. As the denominator's order is third in (6), the number of poles is three. Then, in general, the equation for pole placement can be set as follows:

$$\mathrm{E}_{\mathrm{pole}} = (\mathrm{s}+\omega_1)(s^2 + 2\zeta\omega_2\mathrm{s} + \omega_2^2) \quad (7)$$

where ω_1 and ω_2 are natural frequencies, and ζ is the damping ratio for ω_2. Equation (7) is deemed the general format having three poles since imaginary poles must be complex conjugates.

By comparing (7) with the denominator of (6), (8) can be induced from each coefficient

$$k_1 + k_3 = \omega_1 + 2\zeta\omega_2 \quad \text{(8-a)}$$

$$\omega(\omega - k_2) = \omega_2(\omega_2 + 2\zeta\omega_1) \quad \text{(8-b)}$$

$$k_3\omega^2 = \omega_1\omega_2^2. \quad \text{(8-c)}$$

It can be recognized in (8) that the right-side terms have almost identical formats with the left-side terms. In particular, at (8-b) and (8-c), if ω_2 is equal to the fundamental frequency ω, then the gain setting becomes quite simple. This setting results in

$$k_1 = 2\zeta\omega, \;\; k_2 = -2\zeta\omega_1, \;\; k_3 = \omega_1 \quad (9)$$

$$\frac{\hat{x}}{z} = d(s) = \frac{2\zeta\omega\cdot\mathrm{s}}{s^2 + 2\zeta\omega\cdot\mathrm{s} + \omega^2} \quad \text{(10-a)}$$

$$\frac{\hat{y}}{z} = q(s) = \frac{-2\zeta\omega_1\cdot\mathrm{s}\cdot(s - \omega^2/\omega_1)}{(s^2 + 2\zeta\omega\cdot s + \omega^2)(s+\omega_1)} \quad \text{(10-b)}$$

$$\frac{\hat{D}}{z} = n(s) = \frac{s^2+\omega^2}{s^2 + 2\zeta\omega\cdot\mathrm{s} + \omega^2}\cdot\frac{\omega_1}{s+\omega_1}. \quad \text{(10-c)}$$

The meaning of *d(s)* and *n(s)* can be readily understood in (10). First, *d(s)* is the typical format of a second-order band-pass filter that has center frequency ω and damping ratio ζ. That is, according to *d(s)*, an original signal "z" is band-pass filtered in estimating its ac component "x." As confirmed from (10-a), the property of *d(s)* is not altered by ω_1. Second, *n(s)* is regarded as a low-pass filter cascaded with a notch filter. The notch filter has stop-band at ω while the loss-pass filter has cut-off frequency at ω_1. In general, one low-pass filter may be enough to extract a dc component. However, in ac grids, as the fundamental frequency is not far enough from the dc frequency, a low-pass filter is not enough to filter out "x" from "z." This is why the notch filter is cascaded in (10-c) to estimate the dc component "D." The low-pass filtering in (10-c) is mainly intended for mitigating harmonics.

The meaning of *q(s)* in (10) appears to be complex due to ω_1, contrary to *d(s)* and *n(s)*. Bode plots pertaining to *q(s)* can be helpful to explain the influence of ω_1, as shown in Fig. 1, where ζ is unity for convenience. As shown in the figure, although the magnitude and phase of *q(s)* are not changed at the fundamental frequency ω, the cut-off frequencies can be changed by ω_1. Furthermore, if ω_1 is not equal to ω, a signal amplification

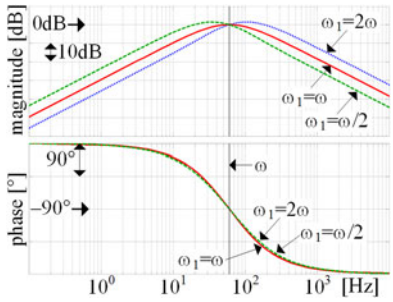

Fig. 1. Bode plot of *q(s)* when ζ is unity.

may arise at the frequencies at which the magnitude response is greater than 0 dB. By this reason, ω_1 is also set as ω. This setting results in (11) from (10). As presented in (11), *q(s)* can be a cascaded combination of *d(s)* and an all-pass filter for phase-shift. In other words, 'y' is estimated such that only its phase deviates by 90° from "x"

$$d(s) = \frac{2\zeta\omega \cdot \mathrm{s}}{s^2 + 2\zeta\omega \cdot \mathrm{s} + \omega^2}, \tag{11-a}$$

$$q(s) = \frac{-2\zeta\omega \cdot \mathrm{s}}{s^2 + 2\zeta\omega \cdot \mathrm{s} + \omega^2} \cdot \frac{s-\omega}{s+\omega} = -d(s) \cdot \frac{s-\omega}{s+\omega}, \tag{11-b}$$

$$n(s) = \frac{s^2 + \omega^2}{s^2 + 2\zeta\omega \cdot \mathrm{s} + \omega^2} \cdot \frac{\omega}{s+\omega} = [1 - d(s)] \cdot \frac{\omega}{s+\omega}. \tag{11-c}$$

In summary, the proposed observer in (4) has multiple filtering functions when considering its transfer functions in (11). Above all, the band-pass filtering denoted by *d(s)* is the foundation of the proposed observer to estimate ac components for grid synchronization. This band-pass filtering mitigates undesirable components at every frequency except ω. In addition, dc rejections for the ac estimations can be confirmed through the final value theorem. As shown in (12), any step variation in "z" is finally eliminated in the ac estimations

$$\lim_{t\to\infty} \hat{x}(t) = \lim_{s\to 0} s \cdot \hat{x}(s) = \lim_{s\to 0} s \cdot d(s) \cdot \frac{z_{\mathrm{DC}}}{s} = 0 \tag{12-a}$$

$$\lim_{t\to\infty} \hat{y}(t) = \lim_{s\to 0} s \cdot \hat{y}(s) = \lim_{s\to 0} s \cdot q(s) \cdot \frac{z_{\mathrm{DC}}}{s} = 0 \tag{12-b}$$

where z_{dc} represents magnitude of a dc component.

There are two gains to be adjustable in (11). First, it is notable that ω is not only an observer gain, but also the fundamental frequency of concern. If this frequency is modified, the pass- and stop-bands of the observer are accordingly moved, as shown in Fig. 2. Thus, by aptly updating ω in real time, the proposed observer can be frequency-adaptive. Second, ζ is associated with the frequency selectivity with respect to ω, as shown in Fig. 3. That is, when the fundamental frequency is fixed at ω, the filtering performances can be enhanced by decreasing the damping ratio ζ, which is generally at the expense of the estimating

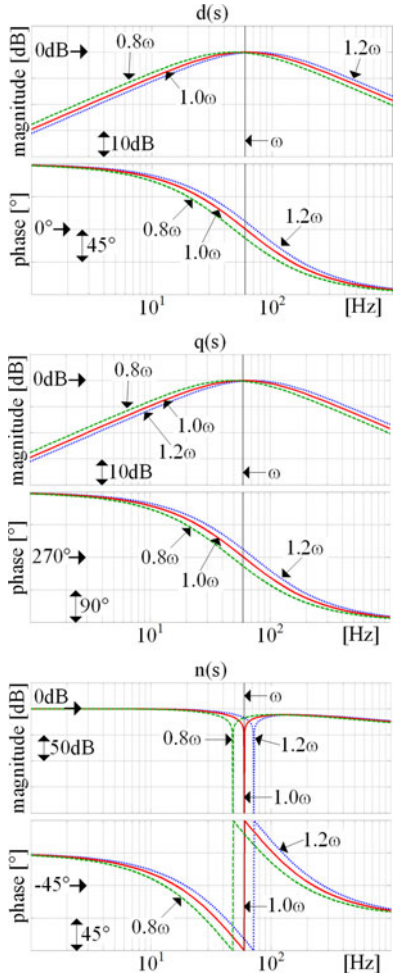

Fig. 2. Bode plots for (11) according to ω with unity ζ.

dynamics. However, it should be noted that the observer responses in terms of ω and ζ are due to the gain setting in which both ω_1 and ω_2 are set as ω. If the gain setting were not based on (7) and (8), another observer responses would be possible.

III. Implementation of PLL

The observer based on (4) can be drawn as a block diagram shown in Fig. 4 when ω_1 and ω_2 are set to ω. From the block diagram, it is recognized that the structure of the proposed observer is very simple. By combining only three integrators, all of the multiple filtering functions explained in (11) are compactly integrated. The utilization of the observer systematically results in this compactness as intended.

In order to check the observer's performance, a dc bias was added to a sinusoidal signal as shown in Fig. 5(a). In the figure, the magnitude of the signal was 1.0 per unit (p.u.) while that of bias was 0.1 pu. When the combined signal is connected to "z" in Fig. 4, the estimated waveforms for "x," "y," and "D" are confirmed in Fig. 5(b) and (c). In conclusion, the proposed observer can extract a quadrature signal as well as the direct signal to the original sinusoidal signal while the dc bias is completely eliminated.

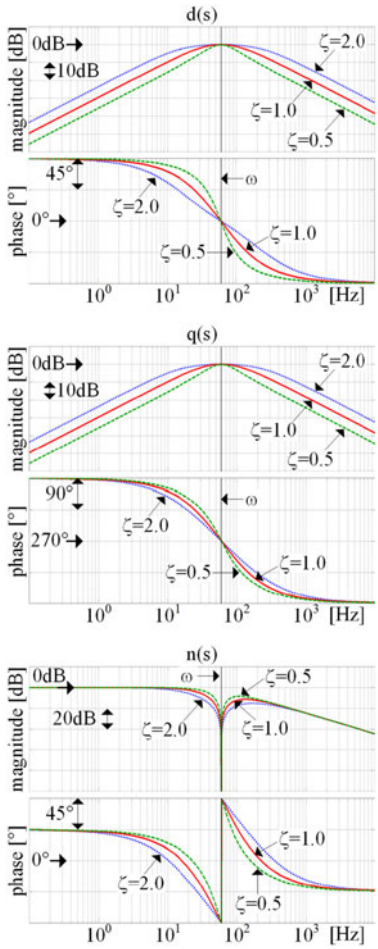

Fig. 3. Bode plots for (11) according to ζ.

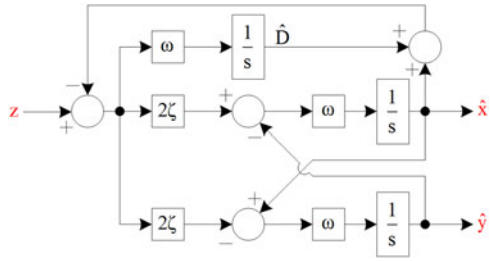

Fig. 4. Frequency-adaptive circle-tracing observer (FACTO).

The direct and quadrature signals compose a circle in their own plane because their magnitude is identical, and their phase difference is 90°. However, the circle's center cannot coincide with the origin of the voltage plane unless dc biases in each signal are perfectly eliminated. By means of the proposed observer, a circle centered at the origin can be traced with a rotating speed. When the gain ω in Fig. 4 is changed, the rotating speed of the traceable circle is changed accordingly. From these properties, the proposed observer is named as frequency-adaptive circle-tracing observer (FACTO).

Before discussing PLL, a step response for the dc estimation can be described. When ω is $2\pi 60$ rad/s and ζ is unity, a step

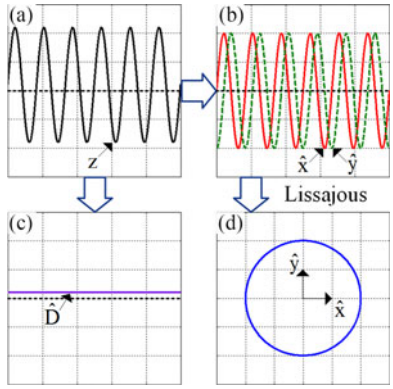

Fig. 5. Operation of FACTO: (0.5 p.u./div and 20 ms/div) in (a)–(c) while (0.5 p.u./div for each axis) in (d).

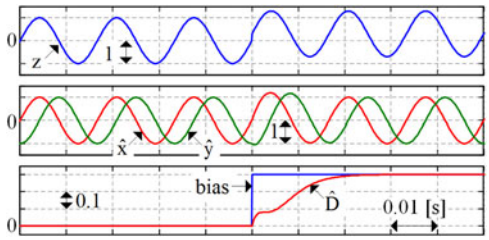

Fig. 6. Transient response of FACTO to a step bias (p.u. for every *y*-axis).

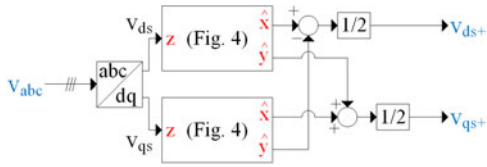

Fig. 7. Utilization of FACTOs to extract positive-sequence voltages.

bias of 0.3 p.u. occurs in Fig. 6. If the notch filtering were absent in (11-c) to estimate a dc bias, the rise time up to 95% would be 8 ms (triple of the time constant). However, the actual rise time was 18 ms because the notch filtering is essentially cascaded with the low-pass filtering. That is, it should be considered that the notch dynamics can slow down the dc estimation.

FACTO can be used for SRF-PLL in single-phase applications because it extracts direct and quadrature voltages. However, this property is also useful in three-phase applications to separate positive-sequence voltages [10]. Specifically, instantaneous positive-sequence voltages can be computed from

$$\begin{bmatrix} v_{\mathrm{ds}+} \\ v_{\mathrm{qs}+} \end{bmatrix} = \frac{1}{2} \begin{bmatrix} d(s) & -q(s) \\ q(s) & d(s) \end{bmatrix} \begin{bmatrix} v_{\mathrm{ds}} \\ v_{\mathrm{qs}} \end{bmatrix} \tag{13}$$

where v_{ds} and v_{qs} are the *d*–*q* voltage in the stationary reference frame, and the subscript "+" indicates positive-sequence. And, *d(s)* and *q(s)* are described in (11).

One example to implement PLL is detailed in Figs. 7–9, which is based on FACTO and (13). Initially, a positive-sequence *d*–*q* voltage, $v_{\mathrm{ds}+}$ and $v_{\mathrm{qs}+}$, can be obtained from a three-phase voltage, v_{abc}, as shown in Fig. 7. After v_{abc} is transformed

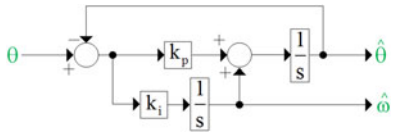

Fig. 8. PLL to estimate angle and frequency.

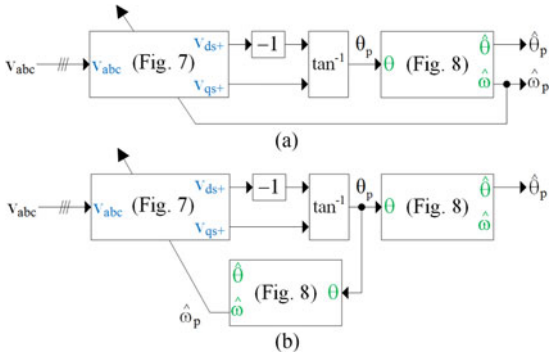

Fig. 9. Entire blocks for grid synchronization with (a) one PLL block (FACTO1) and (b) two PLL blocks (FACTO2).

into $v_{\rm ds}$ and $v_{\rm qs}$, they are respectively sent to their own FACTO blocks. Direct- and quadrature voltages from these FACTOs are then involved in the positive-sequence computation according to (13).

Extraction of a phase angle from positive-sequence voltages, in this paper, is simply based on an arctangent function as shown in (14). It is notified that other methods can be used for this extraction. The relationship between $v_{\rm ds+}$ and $v_{\rm qs+}$ should be carefully recognized in (14). This definition is adopted in this paper because a synchronously rotating reference frame is defined such that positive-sequence voltage vector is aligned with its quadrature-axis

$$\theta_p = \tan^{-1}\left(\frac{-v_{\rm ds+}}{v_{\rm qs+}}\right). \tag{14}$$

An additional usage of PLL appears to be unnecessary as positive-sequence angle can be directly obtained by (14). However, it can be helpful for better performance in grid synchronization. First, the fundamental frequency ω can be estimated by PLL as shown in Fig. 8. This estimated frequency is utilized to update the gains of FACTO for frequency-adaptation in real time. Second, harmonic distortions can be further mitigated by PLL. When a PLL structure is identical to Fig. 8, its estimating responses are derived as (15) [9] and have formats of low-pass filters

$$\frac{\hat{\theta}}{\theta} = \frac{k_p s + k_i}{s^2 + k_p s + k_i} \tag{15-a}$$

$$\frac{\hat{\omega}}{\omega} \approx \frac{k_i}{s^2 + k_p s + k_i} \tag{15-b}$$

$$k_p = 2\zeta_{\rm pll}\omega_{\rm pll}, \quad k_i = \omega_{\rm pll}^2 \tag{15-c}$$

where $\zeta_{\rm pll}$ and $\omega_{\rm pll}$ are damping ratio and bandwidth, respectively.

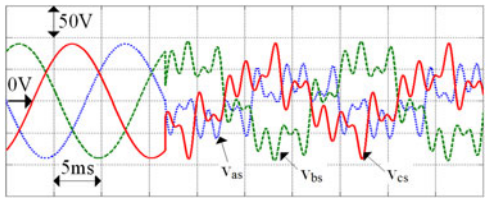

Fig. 10. Fault waveforms for simulations.

A proposed method for grid synchronization is then shown in Fig. 9(a), from grid voltage $v_{\rm abc}$ to estimated angle $\hat{\theta}_p$. In this method, the responses of the angle and frequency estimations must be tied because they share the identical gains as per (15). However, it should be noted that those responses may have to be different for an optimal performance.

Another proposed method is then shown in Fig. 9(b). Even though one more PLL block to implement is essential for this configuration, the estimation responses for angle and frequency can be separately designed. This property is desirable in that the gain updates for FACTOs may be further optimized while not degrading the angle estimation. These two proposed methods are compared in next section, where the former is denoted by FACTO1 while the latter by FACTO2.

IV. Simulation and Experimental Results

A. Simulation Results

Simulations were carried out to evaluate the proposed methods for grid synchronization before experiments. The simulation results are valuable in that the actual grid angle and frequency are correctly identified, which does not in experiments.

All of the control gains for the proposed methods were set such that their responses were similar to those of two conventional methods, SOAP-PLL and DSOGI-FLL [9], [10]. Specifically, the bandwidth for the angle estimation was set to $2\pi 20$ rad/s for FACTO1 of Fig. 9(a), which is identical to the literature [9]. In particular, because the bandwidth for the frequency estimation can be differently set in FACTO2 of Fig. 9(b), it was aptly set to $2\pi 10\,{\rm rad/s}$ while the bandwidth for the angle estimation was $2\pi 20\,{\rm rad/s}$. In addition, all the damping ratios were set to unity.

All of the control blocks were digitally implemented under careful consideration when the sampling frequency was 10 kHz. If the ratio of a sampling frequency to a grid frequency is not large enough, some compensation would be necessary. Given that this issue on digital implementation is out of the scope in this paper, it is not discussed in detail.

For simulations, fault conditions were referred from [21]. When a grid voltage is 110 V–60 Hz, the distortions under fault are given as (16) in per unit. The fault waveforms are shown in Fig. 10

$$V_{1+} = 0.5\angle -30^\circ, \quad V_{1-} = 0.25\angle 110^\circ \tag{16-a}$$

$$V_{5-} = 0.2\angle 0^\circ, \quad V_{7+} = 0.2\angle 0^\circ, \quad V_{11-} = 0.2\angle 0^\circ \tag{16-b}$$

$$f_{\rm fault} - f_{\rm nor} = -5\,{\rm Hz} \tag{16-c}$$

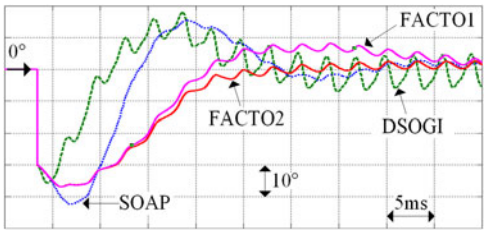

Fig. 11. Angle estimation errors under fault simulation.

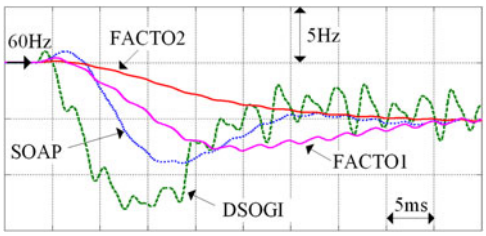

Fig. 12. Frequency estimations under fault simulation.

where subscript numbers represent harmonic orders, and the subscript "−" means negative-sequence. In addition, the grid frequency in normal state and that in fault are denoted by f_{nor} and f_{fault}, respectively.

In response to the fault in Fig. 10, the angle estimation errors are shown in Fig. 11 while the frequency estimations in Fig. 12. When it comes to unbalance and harmonics, the proposed methods present excellent filtering effects comparable to the conventional methods. In particular, the least harmonics are observed in the frequency estimation by FACTO2 because its bandwidth was separately set smaller. When compared to FACTO1, faster settlements are confirmed in FACTO2 for the angle and frequency estimations. That is, it can be thought that the stabilization in the gain updates contributes to the improvement of both the angle and frequency estimations. Hereafter, the proposed method "FACTO" represents only FACTO2. It should be noted that steady-state errors in the estimations were averagely null by the proposed method.

B. Experimental Results

The proposed and conventional methods were also tested in a practical system. The control board was based on TMS320F28335, and the settings for sampling frequency and control gains were identical to those in the simulations. In order to generate a fault situation, an ac programmable source was used in experiments.

Initially, the responses of each method to a dc bias are discussed when a converter is connected to a normal 110V-60 Hz grid. A dc bias was inserted into A-phase voltage on purpose, which was 20% of the nominal magnitude to show evident differences. As a reference, the stationary *d–q* voltage without any filtering is shown in Fig. 13(a). Unlike zero-sequence voltage, the dc bias only at A-phase is not eliminated by the coordinate transformation and affects the voltage estimations in the conventional methods. It is confirmed that the proposed method in

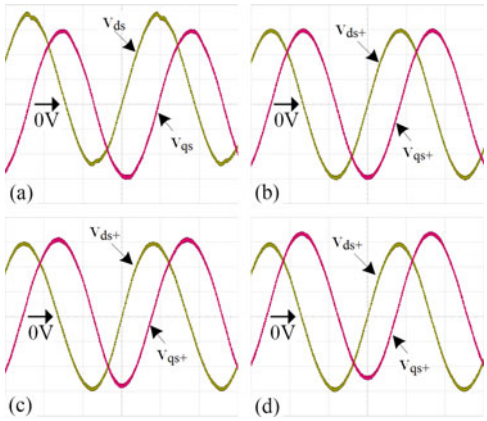

Fig. 13. Positive-sequence estimations under dc bias: (a) raw data, (b) FACTO, (c) SOAP, (d) DSOGI, (30 V/div and 5 ms/div).

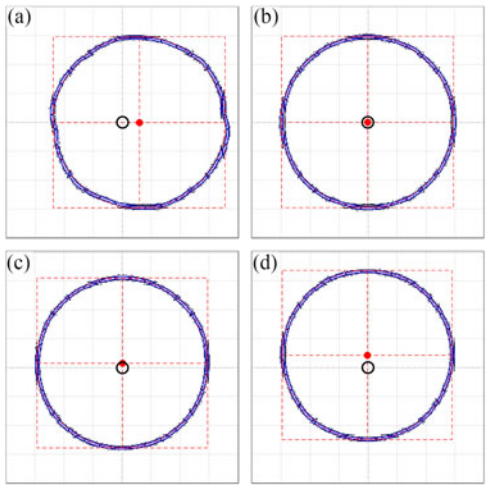

Fig. 14. Positive-sequence traces in voltage plane under dc bias: (a) raw data, (b) FACTO, (c) SOAP, and (d) DSOGI, (30 V/div for each axis).

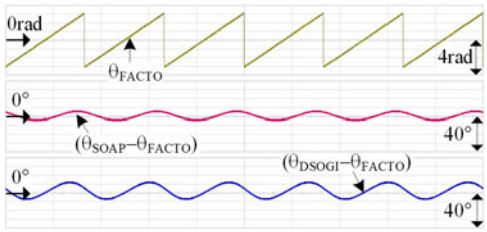

Fig. 15. Angle estimations under dc bias (10 ms/div).

Fig. 13(b) completely rejects the dc bias when compared to the other cases. This rejection can be more conspicuous when the voltages are drawn as Lissajous patterns at the voltage plane, which are shown in Fig. 14. The center of the Lissajous pattern coincides with the origin of the voltage plane only in the proposed method. These figures corroborate the superiority of the proposed method pertaining to dc rejection.

When the grid voltage was the same with Fig. 13(a), the angle and frequency estimations were captured at steady-state as shown in Figs. 15 and 16. In particular, since the actual angle of

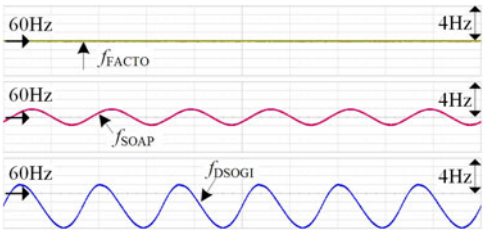

Fig. 16. Frequency estimations under DC bias [10ms/div].

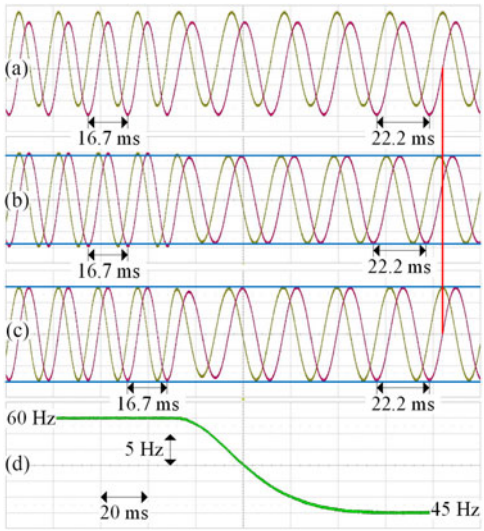

Fig. 17. Voltage estimations under frequency variation: (a) raw data, (b) FACTO with fixed gains, (c) FACTO with gain updates, and (d) estimated frequency by the proposed method.

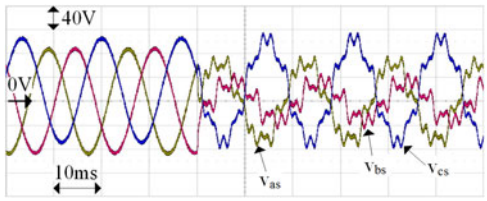

Fig. 18. Fault waveforms in experiments.

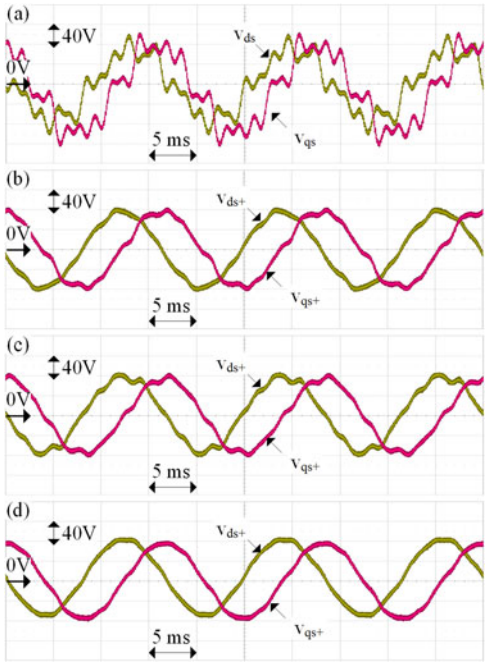

Fig. 19. Voltage estimations in experiments: (a) raw data, (b) FACTO, (c) SOAP, and (d) DSOGI.

the grid voltage cannot be identified in experiments, the angle estimations have been relatively compared with respect to θ_{FACTO} from the proposed method, when considering the simulation results. Initially, given that dc components are transformed into ac components at a synchronous *d–q* reference frame, the influence of the dc bias in Fig. 13(a) appears at the grid frequency in the angle and frequency estimations. Because this frequency is not much higher than the PLL's cut-off frequency, the dc influence is not completely eliminated by SOAP-PLL, as shown in Figs. 15 and 16. However, when compared to DSOGI-FLL, it is confirmed that the PLL can slightly contribute to the dc rejection.

The frequency-adaptation of the proposed method is discussed in Fig. 17 by considering voltage estimations. Under the same conditions with Fig. 13(a), only the grid frequency was abruptly changed from 60 to 45 Hz at once. As shown in Fig. 17(c), the proposed method could finally eliminate the dc bias in spite of the frequency variation. However, the result shown in Fig. 17(b) was obtained by fixing the observer gains in Fig. 7, regardless of the frequency variation. Even with the fixed gains, the dc bias appears to be eliminated. However, in the voltage estimations, the magnitude was decreased and the phase was advanced after the frequency variation. This is mainly caused by a deterioration of the notch filtering detailed in (11-c). It is inferred that the proposed method could be frequency-adaptive by virtue of the gain updates according to Fig. 9(b).

As in the simulations, the grid synchronization methods were tested in experiments under a severe fault situation. Initially, a phase-to-ground fault was made deliberately because it is the most common fault before distribution transformers [23], [24]. In addition, the other faults with respect to unbalance and harmonics were also made at the same time. All of the fault conditions can be referred from the literature [9]. The described fault is then presented in Fig. 18, where a dc bias of 0.2 p.u. is already at C-phase before the fault occurrence.

Under the fault, the positive-sequence *d–q* voltages were estimated as shown in Fig. 19. When it comes to harmonics, all of the estimating methods were good at filtering out. In particular, the least harmonics are observed in the case of DSOGI-FLL. It is noteworthy that the PLL-based methods considered in Fig. 19 have two stages for estimating the angle and frequency. In contrast to DSOGI-FLL, they have one more chance to filter out harmonics in the estimations. However, this additional stage causes a tradeoff between filtering and dynamics.

One option to enhance the filtering with FACTOs is to directly utilize the phase angle from (14) as estimated angle. That is,

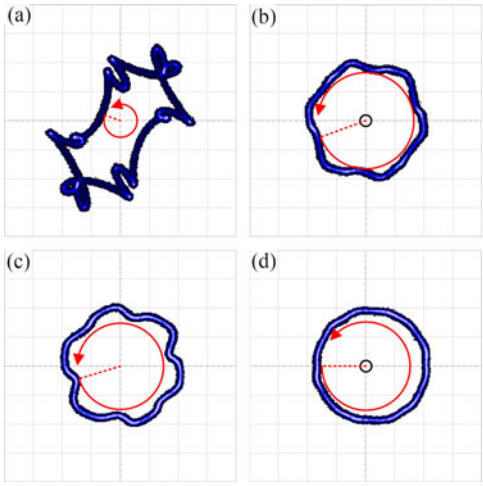

Fig. 20. Positive-sequence traces in voltage plane under fault: (a) raw data, (b) FACTO, (c) SOAP, and (d) DSOGI (40 V/div for each axis).

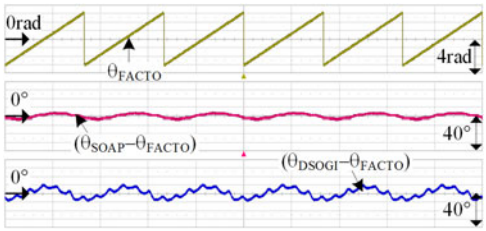

Fig. 21. Angle estimations under fault at 60 Hz (10 ms/div).

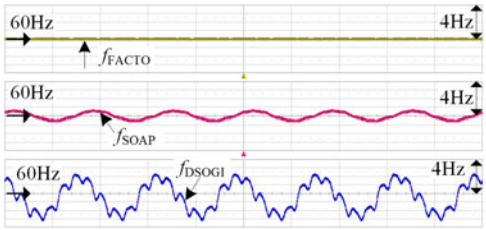

Fig. 22. Frequency estimations under fault at 60 Hz (10 ms/div).

in Fig. 9(b), the PLL for the angle estimation is eliminated while the other PLL is still used for the gain updates. Because the estimating dynamics for angle become faster through this elimination, the filtering in the voltage estimations can be further reinforced by decreasing ζ in Fig. 4 under an intended dynamics. When compared to the DSOGI-based method, this modified method would be beneficial in the dc rejection, which is more evident in Fig. 20. The center of voltage trace does not coincide with the origin by the DSOGI-based method while it does by the FACTO-based method.

The grid synchronization results under the fault are shown in Figs. 21 and 22. When considering Figs. 11 and 12 in addition to Figs. 21 and 22, under similar dynamics, the PLL-based methods have better filtering performances than DSOGI-FLL in the angle and frequency estimations, even though they showed worse filtering performances in the voltage

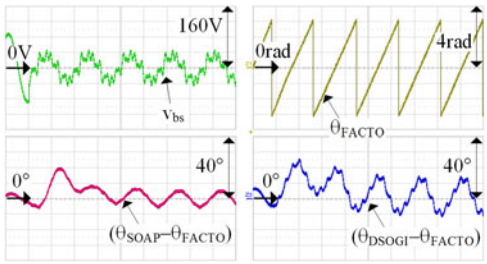

Fig. 23. Transient estimations for angle under fault (10 ms/div).

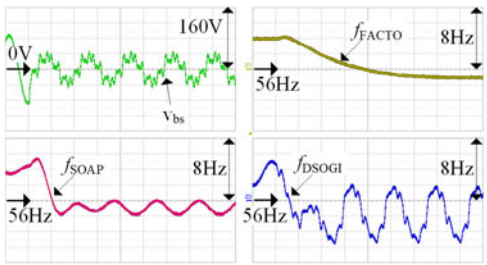

Fig. 24. Transient estimations for frequency under fault (10 ms/div).

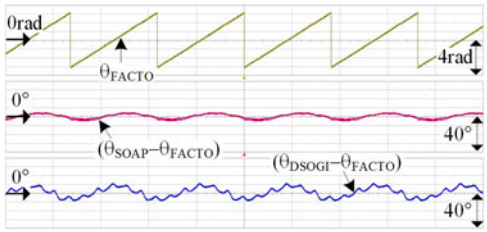

Fig. 25. Angle estimations under fault at 55 Hz (10 ms/div).

estimations. In terms of the unbalance fault, its detrimental effects are not observed in the figures for every method as any distortion at double the grid frequency is negligible. As shown in Figs. 15 and 16, the distortions at the grid frequency from the dc bias are also observed in Figs. 21 and 22 for the conventional methods.

The transient responses are shown in Figs. 23 and 24 when the grid frequency is abruptly decreased by 5 Hz in addition to the fault shown in Fig. 18. These results appear to be different with the simulation results of Figs. 11 and 12 because the phase angle jumps of grid voltages were mainly different at fault occurrence for each case. In spite of this complicated fault, the proposed method could stably carry out the grid synchronization as expected.

After the frequency estimation settles down at 55 Hz, the angle and frequency estimations are shown in Figs. 25 and 26. The average and root-mean-square values with respect to the angle and frequency in Figs. 25 and 26 were virtually identical to those in Figs. 21 and 22. This fact corroborates the frequency adaptiveness of the proposed method, because the conventional methods were proved to be frequency-adaptive and the relative performances of the proposed method were maintained even under the frequency variation.

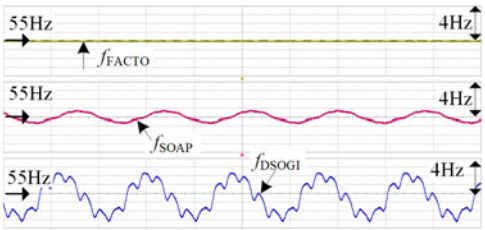

Fig. 26. Frequency estimations under fault at 55 Hz (10 ms/div).

V. Conclusion

In this paper, a grid synchronization method was proposed in basis of a new frequency-adaptive observer. This synchronization method can reject a dc bias in voltage estimations in addition to filtering unbalance and harmonics even if the grid frequency is varying. All of these functions are compactly integrated by virtue of the proposed observer, whose state equation and gain settings were delineated. Finally, the effectiveness of the proposed method has been verified through the comparisons to the conventional methods under diverse grid voltage conditions including dc bias, distortions such as unbalance and harmonics, and frequency variations. This paper has been previously presented in the conference [25].

References

[1] A. E. Emanuel, "Summary of IEEE standard 1459: Definitions for the measurement of electric power quantities under sinusoidal, nonsinusoidal, balanced or unbalanced conditions," *IEEE Trans. Ind. Appl.*, vol. 40, no. 3, pp. 869–876, May/Jun. 2004.

[2] S.-K. Chung, "A phase tracking system for three phase utility interface inverters," *IEEE Trans. Power Electron.*, vol. 15, no. 3, pp. 431–438, May 2000.

[3] S. Golestan, M. Monfared, and F. D. Freijedo, "Design-oriented study of advanced synchronous reference frame phase-locked loops," *IEEE Trans. Power Electron.*, vol. 28, no. 2, pp. 765–778, Feb. 2013.

[4] A. Luna *et al.*, "Grid voltage synchronization for distributed generation systems under grid fault conditions," *IEEE Trans. Ind. Appl.*, vol. 51, no. 4, pp. 3414–3425, Jul./Aug. 2015.

[5] K.-J. Lee, J.-P. Lee, D. Shin, D.-W. Yoo, and H.-J. Kim, "A novel grid Synchronization PLL method based on adaptive low-pass notch filter for grid-connected PCS," *IEEE Trans. Ind. Electron.*, vol. 61, no. 1, pp. 292–301, Jan. 2014.

[6] C. Subramanian and R. Kanagaraj, "Rapid tracking of grid variables using prefiltered synchronous reference frame PLL," *IEEE Trans. Instrum. Meas.*, vol. 64, no. 7, pp. 1826–1836, Jul. 2015.

[7] L. Hadjidemetriou, E. Kyriakides, and F. Blaabjerg, "A new hybrid PLL for interconnecting renewable energy systems to the grid," *IEEE Trans. Ind. Appl.*, vol. 49, no. 6, pp. 1256–1265, Nov./Dec. 2013.

[8] F. Gonzalez-Espin, E. Figueres, and G. Garcera, "An adaptive synchronous-reference-frame phase-locked loop for power quality improvement in a polluted utility grid," *IEEE Trans. Ind. Electron.*, vol. 59, no. 6, pp. 2718–2731, Jun. 2012.

[9] Y. Park, S.-K. Sul, W.-C. Kim, and H.-Y. Lee, "Phase-locked loop based on an observer for grid synchronization," *IEEE Trans. Ind. Appl.*, vol. 50, no. 2, pp. 1256–1265, Mar./Apr. 2014.

[10] P. Rodriguez *et al.*, "A stationary reference frame grid synchronization system for three-phase grid-connected power converters under adverse grid conditions," *IEEE Trans Power Electron.*, vol. 27, no. 1, pp. 99–122, Jan. 2012.

[11] S. Golestan, J. M. Guerrero, and G. B. Gharehpetian, "Five approaches to deal with problem of dc offset in phase-locked loop algorithms: design considerations and performance evaluations," *IEEE Trans. Power Electron.*, vol. 31, no. 1, pp. 648–661, Jan. 2016.

[12] G. Fedele and A. Ferrise, "A frequency-locked-loop filter for biased multi-sinusoidal estimation," *IEEE Trans. Signal Process.*, vol. 62, no. 5, pp. 1125–1134, Mar. 2014.

[13] Y. F. Wang and Y. W. Li, "Grid synchronization PLL based on cascaded delayed signal cancellation," *IEEE Trans. Power Electron.*, vol. 26, no. 7, pp. 1987–1997, Jul. 2011.

[14] F. Gonzalez-Espin, E. Figueres, and G. Garcera, "An adaptive synchronous-reference-frame phase-locked loop for power quality improvement in a polluted utility grid," *IEEE Trans. Ind. Electron.*, vol. 59, no. 6, pp. 2718–2731, Jun. 2012.

[15] S. Golestan, M. Monfared, F. D. Freijedo, and J. M. Guerrero, "Performance improvement of a prefiltered synchronous reference frame PLL by using a PID type loop filter," *IEEE Trans. Ind. Electron.*, vol. 61, no. 7, pp. 3469–3479, Jul. 2014.

[16] W. Li, X. Ruan, C. Bao, D. Pan, and X. Wang, "Grid synchronization systems of three-phase grid-connected power converters: A complex vector-filter perspective," *IEEE Trans. Ind. Electron.*, vol. 61, no. 4, pp. 1855–1870, Apr. 2014.

[17] S. H. Hwang, L. Liu, H. Li, and J. M. Kim, "DC offset error compensation for synchronous reference frame PLL in single-phase grid-connected converters," *IEEE Trans. Power Electron.*, vol. 27, no. 8, pp. 3467–3471, 2012.

[18] M. Karimi-Ghartemani, S. A. Khajehoddin, P. K. Jain, A. Bakhshai, and M. Mojiri, "Addressing DC component in PLL and notch filter algorithms," *IEEE Trans. Power Electron.*, vol. 27, no. 1, pp. 78–86, 2012.

[19] S. Lubura, M. Soja, S. Lale, and M. Ikic, "Single-phase phase locked loop with DC offset and noise rejection for photovoltaic inverters," *IET Power Electron.*, vol. 7, no. 9, pp. 2288–2299, Sep. 2014.

[20] F. Wu, L. Zhang, and J. Duan, "Effect of adding DC-offset estimation integrators in there-phase enhanced phase-locked loop on dynamic performance and alternative scheme," *IET Power Electron.*, vol. 8, no. 3, pp. 391–400, Mar. 2015.

[21] P. Rodriguez *et al.*, "Multiresonant frequency-locked loop for grid synchronization of power converters under distorted grid conditions," *IEEE Trans. Ind. Electron.*, vol. 58, no. 1, pp. 127–138, Jan. 2011.

[22] D. G. Luenberger, "An introduction to observers," *IEEE Trans. Autom. Control*, vol. AC-16, no. 6, pp. 596–602, Dec. 1971.

[23] J. Keller and B. Kroposki, "Understanding fault characteristics of inverter-based distributed energy resources," Nat. Renew. Energy Lab., Golden, CO, USA, Tech. Rep. NREL/TP-550-46698, Jan. 2010.

[24] A. Sannino, M. H. J. Bollen, and J. Svensson, "Voltage tolerance testing of three-phase voltage source converters," *IEEE Trans. Power Del.*, vol. 20, no. 2, pp. 1633–1639, Apr. 2005.

[25] Y. Park, H.-S. Kim, S.-K. Sul, "Frequency-adaptive observer to extract ac-coupled signals for grid synchronization," in *Proc. 9th Int. Conf. ICPE-ECCE Asia.*, Jun. 1–5, 2015, pp. 1188–1194.

Yongsoon Park (S'12–M'15) received the B.S., M.S., and Ph.D. degrees in electrical engineering from Seoul National University, Seoul, South Korea, in 2008, 2010, and 2015, respectively.

From 2015 to 2016, he was a Senior Engineer with Samsung Electronics Co., Ltd., South Korea. Since 2016, he has been with Gwangju Institute of Science and Technology, Gwangju, South Korea, where he is currently an Assistant Professor. His current research interests include design and control of power conversion circuits for grid connection and motor drives.

Hyeon-Sik Kim (S'14) was born in South Korea in 1988. He received the B.S. degree in electrical engineering from Seoul National University, Seoul, South Korea, in 2013, where he is currently working toward the Ph.D. degree.

His current research interests include power electronic control of electric machines and power conversion circuits.

Seung-Ki Sul (S'78–M'87–SM'98–F'00) received the B.S., M.S., and Ph.D. degrees in electrical engineering from Seoul National University, Seoul, South Korea, in 1980, 1983, and 1986, respectively.

From 1986 to 1988, he was an Associate Researcher in the Department of Electrical and Computer Engineering, University of Wisconsin–Madison Madison, WI, USA. From 1988 to 1990, he was a Principal Research Engineer with LG Industrial Systems Company, South Korea. Since 1991, he has been a Member of the Faculty of the School of Electrical and Computer Engineering, Seoul National University, where he is currently a Professor. He has published more than 140 IEEE reviewed journal papers and a total of more than 330 international conference papers in the area of power electronics. His current research interests are control of electrical machines, electric/hybrid vehicles, electric propulsion of ships, and power conditioning systems for renewables. He holds 14 U.S. patents, seven Japanese patents, 11 Korean patents, and 38 Ph.D. degrees have been granted under his supervision.

Prof. Sul was the Program Chair of IEEE PESC'06 and General Chair of IEEE ICPE, ECCE-Asia, 2011. He served as the President of the Korea Institute of Power Electronics in 2015. He has received many best paper awards from international conferences and journals including the first and second best paper awards, from the IEEE TRANSACTIONS ON INDUSTRY APPLICATIONS, both in 2015. He also received the IEEE IAS Outstanding Achievement Award in 2016.